Journal of Applied Surfaces and Interfaces 2 (1-3) (2017) 27-33

Journal homepage: http://revues.imist.ma/?journal=jasi

ISSN: 2550-4800

https://doi.org/10.48442/IMIST.PRSM/jasi-v2i1-3.11217

JASI JOURNAL OF APPLIED SURFACES AND INTERFACES

Synthesis, crystal Structure and temperature induced phase transition in $Ba_{1/5}Sr_{4/5}NiMoO_6$ double perovskite oxide: Study by X-ray diffraction and Raman spectroscopy

M.A. EL Aamrani[1], B. Manoun[1,2,], R. Abkar[1], Y. Tamraoui[1,2], F. Mirinioui[1], A. El Hachmi[1], M. Azrour[3], S. Benmokhtar[4] and P. Lazor[5]*

[1] *Univ. Hassan 1er, Laboratoire des Sciences des Matériaux, des Milieux et de la modélisation (LS3M), 25000, Khouribga, Morocco.*
[2] *Materials Science and Nano-engineering Department, University Mohammed VI Polytechnic, Ben Guerir, Morocco.*
[3] *Laboratoire de Physico-Chimie des Matériaux, Département de Chimie, FST Errachidia, Morocco.*
[4] *LRCPGM, Laboratoire de Recherche de Chimie-Physique Générale des Matériaux, Département de Chimie, Faculté des Sciences Ben M'Sik Casablanca, Maroc.*
[5] *Department of Earth Sciences, Uppsala University, SE-752 36, Uppsala, Sweden*

Received 22 November 2017; Revised 25 December 2017; Accepted 28 December 2017.

Abstract : *$BaCO_3$, $SrCO_3$, NiO, MoO_3 precursors were used as starting materials in the synthesis of double perovskite $Ba_{1/5}Sr_{4/5}NiMoO_6$, and their crystal structure at room tempertaure was solved using X-ray powder diffraction. The Rietveld analysis of X–ray powder diffraction patterns show that both compounds adopt a tetragonal structure with space group I4/m, with unit cell parameters a= 5.58537(1) Å, c=7.9066(2) Å. The structure can be represented as a three-dimensional network of alternating NiO_6 and MoO_6 octahedra, with Ba and Sr atoms occupying the interstitial spaces. Temperature-induced phase transitions of $Ba_{1/5}Sr_{4/5}NiMoO_6$ were investigated by mean of Raman spectroscopy technique at high temperature up to 392 °C. remarkable in the behaviuor of temperature dependence of the modes has been interpreted as a phase transition from the tetragonal (I4/m) to the cubic ($Fm\bar{3}m$) structure.*

Keywords: *$Ba_{1/5}Sr_{4/5}NiMoO_6$; X-ray diffraction; High temperature Raman spectroscopy; phase transition; Rietveld refinements.*

1. Introduction

Double-perovskite oxides with general formula AA'BB'O_6, in which A, and A' are rare earth metal (Ca^{2+}, Sr^{2+} or Ba^{2+}…) and B and B' are transition metal cations, constitute a wide family of materials displaying varied and appealing electronic and magnetic properties. Recently, a few detailed structural studies have shown that double perovskites exhibit diverse properties such as ferroelectricity [1], ferri- and ferromagnetic [2], superconductivity [3] and catalytic properties [4]. The renewed interests in these compounds arise because of the room temperature colossal magneto-resistance [5,6] (CMR) discovery in Sr_2FeMoO_6. In addition to their technological applications, these perovskites have also great crystallographic interest, which is very important for the literature.

Barium and strontium perovskites have revealed a variety of magnetic structures. Thereby, they were the subject of several studies like the study of Ba_2CoWO_6 and Ba_2NiWO_6 [7,8], Ba_2FeReO_6 [9], Ba_2MnReO_6 [10,11], Sr_2FeMoO_6 [12], Sr_2FeTiO_6 [13] and Sr_2NiMoO_6 [14,15]. Also, for the same reason, other researchers have tried to replace some of the barium (or strontium) by strontium (or Barium).

On the other hand, the double perovskites Ba_2NiMoO_6 and Sr_2NiMoO_6 were thoroughly studied by many researchers in the sixties although they were forgotten for more than 30 years [16]. Ba_2NiMoO_6 crystallizes in the cubic system with $Fm\bar{3}m$ (n° 225) space group and has the lattice parameter of a = 8.04 Å [16, 17] and a = 5.54 Å, c = 7.89 Å in Sr_2NiMoO_6 [18, 19]. Concerning this last double perovskite, all the studies that have been made to date have shown that the Sr_2NiMoO_6 crystallizes in the tetragonal system with *I*4/*m* space group [16-18, 20].

Furthermore, the crystallographic phase transitions as a function of temperature are common in this type of perovskite; these transitions are due to the tilting of BO_6/B'O_6 octahedra. Thus, these structural changes are often intimately related to the physical properties of materials. In recent years, many researchers have been interested in the study of double perovskites such as $A_{2-x}A'_xBB'O_6$ (A/A' =Ba, Sr ; B/B' = Co, Ni, Zn / Te, W). Manoun et al [21] report the studies crystal structure stability as function of composition and temperature of $Ba_{2-x}Sr_xMWO_6$ (M= Ni, Co) using X-ray powder diffraction and Raman spectroscopy at elevated temperatures, up to 350°C, the result show that the tetragonal composition has a phase transition induced

* *Corresponding author: E-mail: manounb@gmail.com (Bouchaib MANOUN)*

by the temperature from tetragonal (*I*4/*m*) to cubic ($Fm\bar{3}m$) structure. Also, Nomura and Nakagawa [20] have shown that Sr_2NiMoO_6 has a structure tetragonal at room temperature and a phase transition to cubic occurred at about 230°C. However, according Faik et al. [22], the evolution of the structure Sr_2CrSbO_6 at high temperature shows the presence of two phase transitions $I2/m \rightarrow I4/m \rightarrow Fm\bar{3}m$. Also, according Tamraoui et al. [23], the structure $Ba_{2-x}Sr_xMgTeO_6$ presents the composition-induced phase transition sequence: $I2/m \rightarrow I4/m \rightarrow Fm\bar{3}m$, the monoclinic to tetragonal transition occurs at around 102 °C and the tetragonal to cubic transition at about 303 °C, while Sr_2ZnWO_6 [24] exhibits the $P2_1/n \rightarrow I4/m \rightarrow Fm\bar{3}m$ phase transition sequence.

The main purpose of this work is the synthesis of new double perovskite oxide with general formula $Ba_{1/5}Sr_{4/5}NiMoO_6$ using solid state reaction, the investigation of its crystal structure at room temperature, and phases change at extreme condition of temperature using conventional X-ray diffraction and high temperature Raman spectroscopy techniques as sensitive tools.

2. Experimental procedure

2.1. Solid-state synthesis

Well-crystallized powder sample of $Ba_{1/5}Sr_{4/5}NiMoO_6$ were synthesized using solid state interaction method and many different treatments were applied in order to get single phase for the sample.

Raw materials of $BaCO_3$, $SrCO_3$, NiO, MoO_3 (supplied by Sigma-Aldrich) with >99.9% purity were used to prepare sample. The sample was prepared by using the reaction in a solid state by mixture of all the raw materials. The mixture is ground thereafter in an agate mortar and heated in air in alumina crucible. The following heat treatment procedure was used: The sample was heated to progressively higher temperatures from 100°C to 1300°C with a step of 100°C and periodic intermediate regrinding to improve the homogeneity. Each step lasts 24 hours. After each heating treatment, the sample was cooled down to room temperature, slowly at 5°C/min.

Proper stoichiometric molar ratios of the starting compounds were mixed according to the following chemical reaction:

$$1/5\ BaCO_3 + 4/5\ SrCO_3 + NiO + MoO_3 \xrightarrow{\Delta(1200\,^{\circ}C)\ \text{in Air}} Ba_{1/5}Sr_{4/5}NiMoO_6 + 2CO_2$$

2.2. XRD measurements

The final product of $Ba_{1/5}Sr_{4/5}NiMoO_6$ have been controlled by X-ray powder diffraction analysis using a D2 PHASER diffractometer, with the Bragg–Brentano geometry, using Cu Kα radiation (λ=1.5418 Å) with 30 KV and 10 mA, Soller slits of 0.02 rad on incident and diffracted beams; divergence slit of 0.5°; antiscatter slit of 1°; receiving slit of 0.1 mm; with sample spinner, and a Lynxeye detector type with a maximum global count rat >1000.000.000 cps. The pattern was scanned through steps of 0.010142° (2θ), between 15 and 105° (2θ) with a fixed-time counting of 2 seconds/step.

The dataset were analyzed by the Rietveld method using the Fullprof program [25] integrated in Winplotr software [26]. The Rietveld refinement of the observed powder XRD data is initiated with scale and background parameters and successively other profile parameters are included. The background is fitted with a fifth order polynomial. The peak shape is fitted with a pseudo-Voigt profile function. After an appreciable profile matching the position parameters and isotropic atomic displacement parameters of individual atoms were also refined.

2.3. Raman spectroscopy

Experiments have been carried out using Raman spectroscopic system designed and built at the Department of Earth Sciences, Uppsala University [27,28]. The key system components include a high-throughput, single stage imaging spectrometer (HoloSpec f/1.8i, Kaiser Optical Systems, Inc.) equipped with a holographic transmission grating and thermoelectrically cooled two-dimensional multichannel CCD detector (Newton, Andor Technology, 1600×400 pixels, thermoelectrically cooled down to -60°C), an argon-ion laser (Spectra-Physics, 514.5nm, 20mW), and an optical imaging system (magnification 20×, spatial resolution~1μm). Two holographic notch filters (Kaiser Optical Systems, Inc.) blocked the Rayleigh line. The spectrometer was calibrated by fluorescence lines of the neon lamp. Non-polarized Raman spectra were collected in the back-scattering geometry, in the range 180–2280cm^{-1}, at a resolution of about 3cm^{-1}. Accuracy and precision of spectral measurements, as estimated from the wavelength calibration procedure and peak fitting results, were 1.5cm^{-1} and 0.1– 0.4cm^{-1}, respectively. The acquisition time varied from 30s to 5min.

Heating was accomplished by using a mica insulated band heater (DuraBand, Tempco Electric heater Corporation) mounted around the sample ceramic holder and connected to a variable transformer. Temperature changes during the heating/cooling cycles were induced and controlled by adjusting the transformer's voltage (0-240V) and monitored with an accuracy of ±1°C by the K-type thermocouple adjacent to the sample. During the spectral acquisitions, temperatures were stabilized to within 1 and 3°C, for the low and high temperature measurements, respectively.

3. Results and discussion

3.1. Crystal structure at room temperature

Fig.1 shows the final plots of the observed and calculated profiles at ambient temperature. While Table 1 collects the details of Rietveld refinement parameters for $Ba_{1/5}Sr_{4/5}NiMoO_6$-tetragonal phase. In order to solve the crystal structure of this compound an indexing of X-ray powder diffraction pattern was performed by means of the computer program Dicvol [29]. The first 15 peak positions, with a maximal absolute error of 0.03°(2θ), were used as input data. The X-ray diffraction pattern was assigned to a tetragonal symmetry with (*I*4/*m*) as a space group. The lattice parameters that were refined using the complete powder diffraction data sets are listed in Table 1.

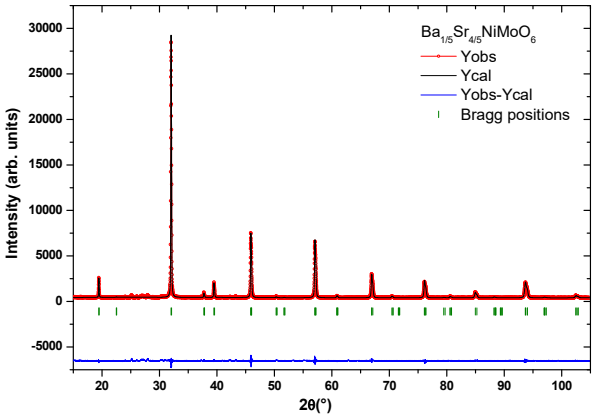

Fig.1. *Final Rietveld plots for $Ba_{1/5}Sr_{4/5}NiMoO_6$. The upper symbols illustrate the observed data (circles) and the calculated pattern (solid line). The vertical markers show calculated positions of Bragg reflections. The lower curve is the difference diagram. The non-indexed peaks are unidentified.*

The following structural and instrumental parameters were refined from the XRD data: scale factor, background coefficients, zero-point error, unit-cell parameters, pseudo-Voigt corrected for asymmetry parameters, Caglioti parameters (U, V, and W), atomic positions, and an overall isotropic thermal factor. The starting data needed for Rietveld refinements are the atomic positions and unit cell parameters, the model was taken from work reported by Y. Tamraoui et al. [23]. In this model Ba^{2+}/Sr^{2+}, Ni^{2+} and Mo^{6+} are placed at 4d(0, 1/2, 1/4), 2a(0, 0,0) and 2b(0, 0, 1/2) sites, respectively. There are two crystallographically distinct oxygen atoms O1(0,0,z) and O2(x,y,0), present in the unit cell.

The refinements of the occupancies of all the atoms show no significant deviation from their stoichiometric values. Significantly good residuals of the refinements are obtained. The refined position coordinates along with other crystallographic data are given in Table 2.

Table 1

Details of Rietveld refinement conditions for $Ba_{1/5}Sr_{4/5}NiMoO_6$ tetragonal-phase.

	$Ba_{1/5}Sr_{4/5}NiMoO_6$
Symmetry	Tetragonal
Wavelength (Å)	λkα1=1.5406
Step scan increment (°2θ)	0.010142
2θ range (°)	15-105
Program	FullProf
Zero point (°2θ)	0.0312
Pseudo-Voigt function PV = ηL + (1-η)G	η=0.54
Caglioti parameters	U=0.090 V= -0.019 W=0.008
No. of reflections	86
No. of refined parameter	23
Space group	*I*4/*m*
a (Å)	5.5854(1)
c (Å)	7.9066(2)
V ($Å^3$)	246.66(1)
Atom number	5
RF	3.81
RB	3.14
Rp	4.62
Rwp	6.25
cRp	4.17
cRwp	5.35

Table 2

Details of Rietveld refinement conditions of the tetragonal $Ba_{1/5}Sr_{4/5}NiMoO_6$ tetragonal-phase.

Atom	x	y	z	B(Å²)	Occ.
Mo	0	0	0.5	0.473(4)	1
Ni	0	0	0	0.647(7)	1
Ba/Sr	0	0.5	0.25	0.639(3)	0.4/1.6
O1	0	0	0.2595(1)	0.913(1)	2
O2	0.2522(3)	0.2899(8)	0	0.913(1)	4

The analysis of refined crystallographic parameters indicates that Ni^{2+} and Mo^{6+} cations are octahedrally coordinated with the oxygen atoms. The NiO_6 and MoO_6 octahedra are alternatively connected and extended in three dimensions. The O(2) atoms connect the NiO_6 and MoO_6 octahedra along the c-axis. In ab-plane NiO_6 and MoO_6 octahedra are connected through the O(1) atoms. The typical Ni–O(1)–Mo bond angle constrained to 180° by space group I4/m and O(1) position coordinates (0,0,z), indicating no tilt with respect to c-axis. The appreciable tilt of the octahedra is observed from the Ni–O(2)–Mo bond angle (169°). The tilt pattern of the octahedral units satisfies the ($a^+a^+c^-$) tilt system in Glazer's notation [30,31]. A (001) projection indicating the typical polyhedral arrangement and the tilt pattern is shown in Fig.2. In Fig.3 we illustrate the Ba/Sr environment.

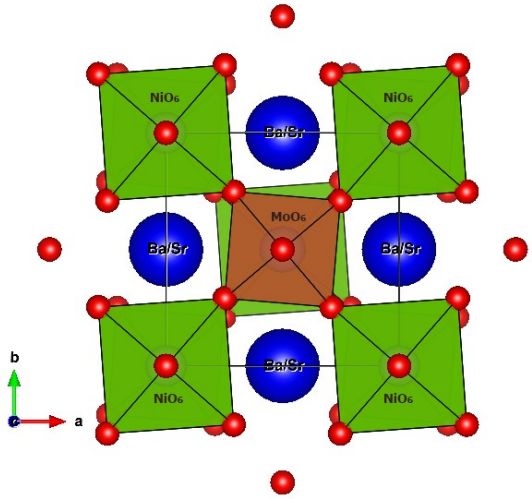

Fig.2. *Illustrations of the effect of tilting of the NiO_6 and MoO_6 octahedra in tetragonal structure.*

The analysis of various inter-atomic distances (Table 3) shows that Ba/Sr atoms form Ba/SrO_{12} polyhedra with the Ba/Sr–O bond lengths ranging between 2.66 and 2.93Å, and the average d value is approximately 2.80Å. The Ni^{2+} and Mo^{6+} have octahedral coordination with the Ni–O bond lengths ranging between 2.09 and 2.13Å and the Mo–O bonds lengths ranging between 1.81 and 1.87 Å.

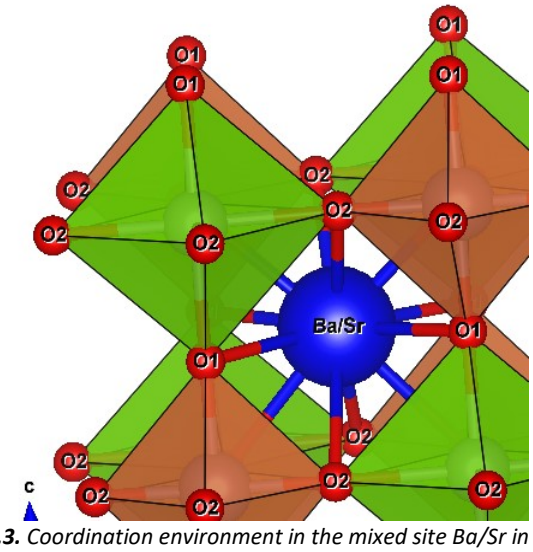

Fig.3. *Coordination environment in the mixed site Ba/Sr in tetragonal structure.*

Note that the distances of Mo–O are considerably shorter than expected (1.99 Å) from the Shannon ionic radii of Mo^{6+} (0.59Å) and O^{2-} (1.4 Å). The Ni–O values are very close to what is expected: 2.09Å. Tamraoui et al. [23], have shown in a study of substitution of Ba^{2+} by Sr^{2+} in $Ba_{2-x}Sr_xMgTeO_6$ ($0 \leq x \leq 2$) double perovskites, that the distances Te-O contracts when the substitution of Ba^{2+} by Sr^{2+} becomes very important, and that as the amount of strontium increases in the different compositions, Te-O decreases from a critical value of x. And for the same reasons, the short distances obtained for Mo-O are due to the fact that strontium occupies a large part of A sites in $A_2BB'O_6$. This contraction is not due to the cation Ni^{2+} since this one entirely occupies the site of B while Mo^{6+} occupies the site of B'.

The observed tolerance factor, calculated from the distances obtained from the Rietveld refinements, can be written, for double perovskites with mixed A-site $A_{2-x}A'_xBB'O_6$, as [32]:

$$t = \frac{\left(\frac{2-x}{2}\right).r_A + \frac{x}{2}.r'_A + r_O}{\sqrt{2}.\left(\frac{r_B + r_{B'}}{2} + r_O\right)}$$

Where r_A, $r_{A'}$, r_B, and $r_{B'}$ are the ionic radii of the respective ions.

It is worth noting that based on the various inter-atomic distances (Table 3) the calculated t of $Ba_{1/5}Sr_{4/5}NiMoO_6$ is 0.9987, which is in agreement with our choice of system and space group, since for a tetragonal structure with a space group *I*4/*m*, the tolerance factor is between 1.00> t >0.97 [33].

Table 3

Selected inter-atomic distances (Å), O-Mo-O angles and the observed tolerance factor for $Ba_{1/5}Sr_{4/5}NiMoO_6$.

2× Mo-O1 4× Mo-O2 <Mo-O>	1.900(9) 1.820(3) 1.8466
2× Ni-O1 4× Ni-O2 <Ni-O>	2.050(9) 2.150(3) 2.1166
4 × Ba/Sr-O1 4 × Ba/Sr-O2 4 × Ba/Sr-O2 <Ba/Sr-O>	2.794(2) 2.690(2) 2.910(2) 2.798
O1-Mo-O1 O1-Mo-O2 O2-Mo-O2 O2-Mo-O2 Tolerance factor	180 90 90 180 0.9987

3.2. Group theory analysis of structural Raman-active modes

The site symmetry group analysis performed for *I*4/*m* space group leads to the irreducible representation given in the Table 4.

Among all of these modes predicted by the theory, only A_g, B_g and E_g are Raman-active modes. According to the factor group [34] analysis, nine Raman-active modes should be observed for the *I*4/*m* structure. Most of the bands are weak; there are only three strong bands and they are observed around 450, 560 and 820cm^{-1}.

Since the $Ba_{1/5}Sr_{4/5}NiMoO_6$ specimens are polycrystalline powder, we cannot precisely assign the Raman modes in the tetragonal phase (*I*4/*m*). However, and taking into account the results obtained by Liegeois-

Duyckaerts et al. [35], the observed Raman modes can be classified into three general families of lattice vibrations: Ba^{2+}/Sr^{2+} translations, as well as translational and rotational modes of the MoO_6-octahedra, at wavenumbers below 200cm^{-1}; O–Mo–O bending vibrations, in the 200-500 cm^{-1} region; and Mo–O stretching modes, at wavenumbers over 500cm^{-1}.

Table 4

Factor group analysis for $Ba_{1/5}Sr_{4/5}NiMoO_6$ at room temperature.

Atom	Site	Sym.	Distribution
Ba/Sr	4d	*-4*	$A_u + B_g + {}^1E_g + {}^1E_u + {}^2E_g + {}^2E_u$
Ca	2a	*4/m*	$A_u + {}^1E_u + {}^2E_u$
Te	2b	*4/m*	$A_u + {}^1E_u + {}^2E_u$
O1	4e	*4*	$A_g + Au + {}^1E_g + {}^1E_u + {}^2E_g + {}^2E_u$
O2	8h	*m*	$2A_g + Au + 2Bg + {}^1E_g + 2{}^1E_u + {}^2E_g + 2{}^2E_u$
$\Gamma = 3A_g + 5Au + 3Bg + 3{}^1E_g + 6{}^1E_u + 3{}^2E_g + 6{}^2E_u$ $\Gamma^{acoustic} = A_u + {}^1E_u + {}^2E_u$ $\Gamma^{Raman} = 3A_g + 3Bg + 3{}^1E_g + 3{}^2E_g$ $\Gamma^{IR} = 4A_u + 5{}^1E_u + 5{}^2E_u$			

3.3. Temperature study of $Ba_{1/5}Sr_{4/5}NiMoO_6$ double perovskites

Raman spectra of $Ba_{1/5}Sr_{4/5}NiMoO_6$ were collected in-situ at room-pressure and elevated temperatures, up to 392°C. The Raman spectra obtained at several temperatures are presented in Fig.4. In Fig.5 we illustrate the mode 820 cm^{-1} as a function of the temperature. Clear changes were observed in the curves showing the tetragonal to the cubic phase transition. The temperature dependence of the modes, the intensity ratio and the Full Width at Half Maximum (FWHM) are presented in Fig.6 and Fig.7.

The strongest temperature changes in wavenumbers we observed are for modes recorded around, 450cm^{-1}, 560 cm^{-1} and 820 cm^{-1}.

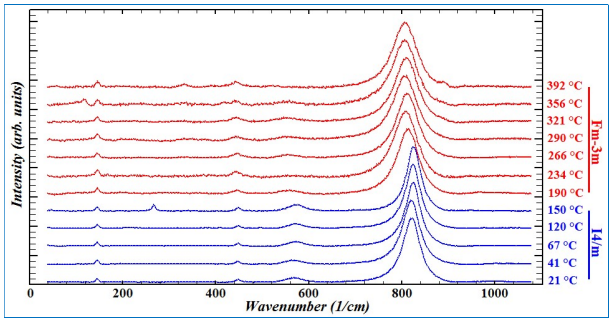

Fig.4. *The Raman spectra of $Ba_{1/5}Sr_{4/5}NiMoO_6$ obtained for selected temperatures, as indicated.*

All lattice modes show a monotonous change in wavenumbers while temperature is increased. The transition from the tetragonal phase to the cubic phase shows considerable changes in the temperature dependence of the modes observed around at 450cm^{-1}, 560cm^{-1} and 820cm^{-1}.

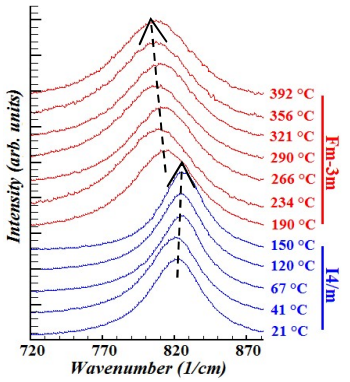

Fig.5. *Raman modes for 820 cm^{-1} mode as a function of the temperature.*

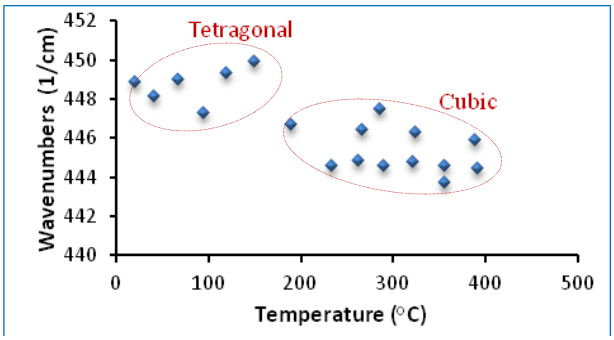

Fig.6a. *Raman modes for 450 cm^{-1} mode as a function of temperature.*

Remarkable changes in the temperature dependence of the modes are observed for the positions of modes centered at 450 cm^{-1} and at 820cm^{-1} (Fig.6a & Fig.6b); likewise, the FWHM and the intensity ratio of Raman modes 820 cm^{-1} and 560 cm^{-1} (Fig.7a & Fig.7b) show a change in the slope at around 190°C, indicating the phase transition from the tetragonal (*I*4/*m*) to cubic ($_{F\,m\,\bar{3}\,m}$) structure.

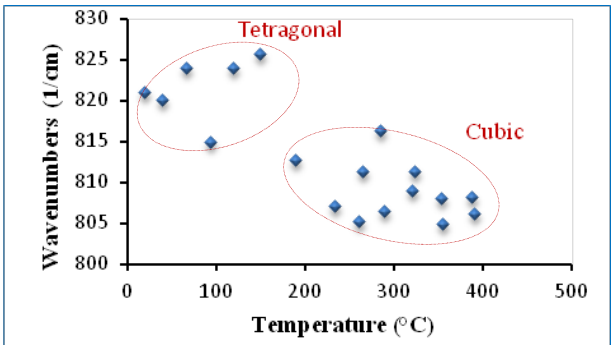

Fig.6b. *Raman modes for 820 cm^{-1} mode as a function of temperature.*

The main difference between the high temperature structure and the low temperature one is the rotation of the NiO_6 and MoO_6 octahedra around the tetragonal axes in the tetragonal phases. These distortions most likely occur due to the competing bonding preferences of the Ba/Sr and Ni site ions. At high temperatures, both

the expanded cell and the greater thermal motion of the atoms, allow those to form a cubic cell. However, on cooling the increased bond strain drives the tetragonal distortion.

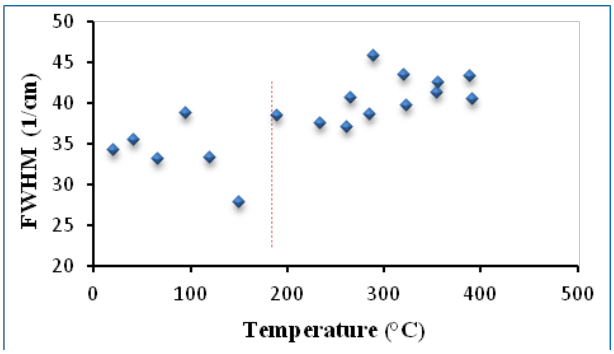

Fig.7a. *FWHM (cm^{-1}) for 820cm^{-1} mode as a function of temperature, the change in the slope shows the phase transition occurrence.*

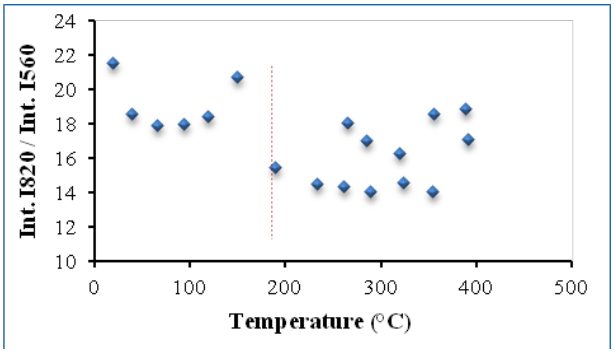

Fig.7b. *Intensity ratio variation I820/I560 as a function of temperature, the change in the slope shows the phase transition occurrence.*

4. Conclusion

In this study, using the X-ray diffraction and Raman spectroscopy techniques, we reported on the crystal structure and on the high temperature induced phase transition in $Ba_{1/5}Sr_{4/5}NiMoO_6$ double perovskite oxide. This study has been done on powder sample. At room temperature, the compound crystallize in a tetragonal system with the space group *I*4/*m*. Increasing the temperature leads to considerable changes in the temperature dependence of the Raman modes. When the temperature reached around 190°C, a large change is observed; thus, showing the transition from the tetragonal (*I*4/*m*) phase to the cubic ($Fm\bar{3}m$) phase. For this oxide, structural symmetry change is clearly revealed by changes in the temperature linear dependencies of the Raman modes which exhibit a discontinuous alteration of their slopes upon the transition.

Acknowledgements

The authors are grateful to the Office Chérifien des Phosphates in the Moroccan Kingdom (OCP group) and Mohammed VI Polytechnic University, the University Hassan 1st for its support and the Swedish Research Council for the financial grant SRL (MENA) # 348- 2014-4287.

References

[1] C. Ederer, A.N. Spaldin. Current Opinion in Solid State and Materials Science 9(3) (2005) 128-139,
[2] J.B. Goodenough, J.M. Longo, Condensed Matter 4 (1970) 126-129.
[3] R.J. Cava, B. Batlogg, J.J. Krajewski, R. Farrow, L.W. Rupp, A.E. White, K. Short, W.F. Peck, T. Kometani, Nature 332 (1988) 814–816.
[4] M. Misono, Catalysis Today 144(3-4) (2009) 285–291.
[5] T. Burnus, Z. Hu, H.H. Hsieh, V.L.J. Joly, P.A. Joy, M.W. Haverkort, H. Wu, A. Tanaka, H.-J. Lin, C.T. Chen, L.H. Tjeng, Physical Review B 77 (2008) 125-124.
[6] J.J. Capponi, C. Chaillout, A.W. Hewat, P. Lejay, M. Marezio, N. Nguyen, B. Raveau, J.L. Soubeyroux, J.L. Tholence, R. Tournier, Europhysics Letters 3 (1987) 1301-1307.
[7] G. Blasse, Journal of Inorganic and Nuclear Chemistry 27 (1965) 993-1003.
[8] D.E. Cox, G. Shirane, B.C. Frazer, Journal of Applied Physics 38 (1967) 1459-1460
[9] W. Prellier, V. Smolyaninova, A. Biswas, C. Galley, R.L. Greene, K. Romesa, J Gopalakrishnan, Journal of Physics: Condensed Matter 12 (2000) 965–973.
[10] C.P. Khattak, D.E. Cox, F.F.Y. Wang, Journal of Solid State Chemistry 13 (1975) 77-83.
[11] A.W. Sleight, J.F. Weiher, Journal of Physics and Chemistry of Solids 33 (1972) 679-687.
[12] G. King, A. Wills, P. M. Woodward, Physical Review B79 (2009) 224-228.
[13] G. King, S. Thimmaiah, A. Dwivedi, P.M. Woodward, Chemistry of Materials 19(26) (2007) 6451–6458.
[14] A.K. Azad, S.A. Ivanov, S.-G. Eriksson, J. Eriksen, H. Rundlöf, R. Mathieu, P. Svedlindh, Materials Research Bulletin 36 (2001) 2215–2228.
[15] V.V. Gagulin, S. K. Korchagina, V. V. Ivanova, and A. Yu. Shevchuk, Inorganic Materials 39(6) 2003 625–626.
[16] J. Maria, M.L. José, A. Alonso, M.T. Casais, European Journal of Inorganic Chemistry 15 (2003) 2839-2844.
[17] A.K. Eriksson, S.G. Eriksson, S.A. Ivanov, C.S. Knee, J. Eriksen, H. Rundlöf, M. Tseggai, Materials Research Bulletin 41 (2006) 144-157.
[18] M.W. Lufaso, R.B. Macquart, Y. Lee, T. Vogt, H.C. zur Loye, Journal of Physics: Condensed Matter 18 (2006) 8761–8780.
[19] A. Prasatkhetragarn, S. Kaowphong, R. Yimnirun, Applied Physics A 107 (2012) 117-121.
[20] S. Nomura, T. Nakagawa1, Journal of the Physical Society of Japan 21 (1966) 1068-1071.
[21] B. Manoun, A. Ezzahi, S. Benmokhtar, L. Bih, Y. Tamraoui, R. Haloui, F. Mirinioui, S. Addakiri, J.M. Igartua, P. Lazor, Journal of Molecular Structure 1045 (2013) 1–14.
[22] A. Faik, J. M. Igartua, M. Gateshki, G.J. Cuello, Journal of Solid State Chemistry 182 (2009) 1717–1725.
[23] Y. Tamraoui, B. Manoun, F. Mirinioui, R. Haloui, P. Lazor, Journal of Alloys and Compounds 603 (2014) 86–94.
[24] B. Manoun, J. M. Igartua, P. Lazor, A. Ezzahi, Journal of Molecular Structure 1029 (2012) 81–85.
[25] J. Rodriguez-Carvajal, Collected Abstracts of Powder Diffraction Meeting, Toulouse (France) (1990) 127.

[26] T. Roisnel, J. Rodriguez-Carvajal, Materials Science Forum 378 (2001) 118.
[27] M. Azdouz, B. Manoun, M. Azrour, L. Bih, L. El Ammari, S. Benmokhtar, P. Lazor, Journal of Molecular Structure 963 (2010) 258-266.
[28] H. Bih, L. Bih, B. Manoun, M. Azdouz, S. Benmokhtar, P. Lazor, Journal of Molecular Structure 936 (2009) 147-155.
[29] A. Boultif, D. Louër, Journal of Applied Crystallography 24 (1991) 987-993.
[30] A.M. Glazer, Acta Crystallographica B28 (1972) 3384-3392.
[31] A.M. Glazer, Acta Crystallographica A 31 (1975) 756-762.
[32] G. Popov, M. Greenblatt, Physical Review B67 (2003) 024406.
[33] D. Serrate, J.M. De Teresa, M.R. Ibarra, Journal of Physics: Condensed Matter 19(2) (2007) 023201.
[34] E. Kroumova, M.I. Aroyo, J.M. Perez-Mato, A. Kirov, C. Capillas, S. Ivantchev, H. Wondratschek, Phase Transition 76 (2003) 155–170.
[35] M. Liegeois-Duyckaerts, P. Tarte, Spectrochimica Acta Part A: Molecular Spectroscopy 30 (1974) 1771-1786.